Monitoring blood-brain barrier integrity following amyloid-β immunotherapy using gadolinium-enhanced MRI in a PDAPP mouse model

Reference:

Blockx Ines, Einstein Steve, Guns Pieter-Jan, van Audekerke Johan, Guglielmetti Caroline, Zago Wagner, Roose Dimitri, Verhoye Marleen, Van Der Linden Anne-Marie, Bard Frederique.- Monitoring blood-brain barrier integrity following amyloid-β immunotherapy using gadolinium-enhanced MRI in a PDAPP mouse model

Journal of Alzheimer's disease - ISSN 1387-2877 - 54:2(2016), p. 723-735

Full text (Publishers DOI): http://dx.doi.org/doi:10.3233/JAD-160023

Title: Monitoring Blood Brain Barrier Integrity Following Abeta Immunotherapy Using Gadolinium-enhanced MRI in a PDAPP Mouse Model.

Authors:

Ines Blockx[a*], Steve Einstein[b*], Pieter-Jan Guns[a,d], Johan Van Audekerke[a], Caroline Guglielmetti[a], Wagner Zago[e], Dimitri Roose[a], Marleen Verhoye[a], Annemie Van der Linden[a] and Frederique Bard [c#]

Affiliations:

(a) Bio-Imaging Lab, University of Antwerp, Antwerp, Belgium

(b) Janssen Research and Development, Titusville, NJ, USA

(c) Janssen Prevention Center, San Diego, CA, USA.

(d) Expert Group Antwerp Molecular Imaging (EGAMI), University of Antwerp, Antwerp, Belgium

(e) Prothena Biosciences Inc, South San Francisco, CA

Running title: BBB integrity in a PDAPP Mouse Model.

[*] Both authors equally contributed to the manuscript.

[#]To whom correspondence should be addressed: Frédérique Bard, Janssen Prevention Center, San Diego, CA, USA.

E-mail: fbard@its.jnj.com

Tel: (1) 858 320 3323

Keywords: Neuroimaging; transgenic mouse model; Alzheimer's disease, Blood-Brain Barrier (BBB), immunotherapy

Abstract

Background: Amyloid-related imaging abnormalities (ARIA) have been reported with some anti-Aβ immunotherapy trials. They are detected with magnetic resonance imaging (MRI) and thought to represent transient accumulation of fluid/edema (ARIA-E) or microhemorrhages (ARIA-H). Although the clinical significance and pathophysiology are unknown, it has been proposed that anti-Aβ immunotherapy may affect blood-brain barrier (BBB) integrity.

Objective: To examine vascular integrity in aged (12-16 months) PDAPP and wild type mice (WT), we performed a series of longitudinal *in vivo* MRI studies.

Methods: Mice were treated on a weekly basis using anti-Aβ immunotherapy (3D6) and follow up was done longitudinally from 1-12 weeks after treatment. BBB-integrity was assessed using both visual assessment of T_1-weighted scans and repeated T_1 mapping in combination with gadolinium (Gd-DOTA).

Results: A subset of 3D6 treated PDAPP mice displayed numerous BBB disruptions, whereas WT and saline treated PDAPP mice showed intact BBB integrity under the conditions tested. In addition, the contrast induced decrease in T_1 value was observed in the meningeal and midline area. BBB disruption events occurred early during treatment (between 1 and 5 weeks), were transient, and resolved quickly. Finally, BBB-leakages associated with microhemorrhages were confirmed by Perls' Prussian blue histopathological analysis.

In conclusion, our preclinical findings support the hypothesis that 3D6 leads to transient leakage from amyloid-positive vessels. The current study has provided valuable insights on the time course of vascular alterations during immunization treatment and supports further research in relation to the nature of ARIA and the utility of *in vivo* repeated T_1 MRI as a translational tool.

Keywords

Alzheimer's disease; immunotherapy; MRI; ARIA; BBB; mouse model

Introduction

Alzheimer's disease (AD) is the most common cause of dementia and represents an unprecedented public health problem. Although much of the underlying biological mechanisms leading to AD are still unclear, the amyloid hypothesis has tremendously influenced research conducted in both academic and pharmaceutical settings [1]. Since the accumulation of Aβ is generally believed to play a causative role in AD, the development of disease-modifying drugs aiming at reducing the Aβ levels in the brain has been a priority for many pharmaceutical companies. A number of reports have shown that active and passive Aβ immunotherapeutic approaches are effective in reducing brain Aβ animal [2-6] and in clinical studies [7, 8]. Bapineuzumab, a humanized form of the murine monoclonal antibody 3D6, recognizes the N-terminus of Aβ and binds all forms of Aβ (e.g. monomer, prefibrillar aggregates, and plaques) [9]. Bapineuzumab (and 3D6) is believed to clear Aβ centrally through both microglial phagocytosis [5] and neutralization of soluble aggregates [9]. In several Aβ immunotherapy clinical trials, abnormalities have been detected by brain MR imaging [10, 11] - so called Amyloid-Related Imaging Abnormalities (ARIA) [12]. ARIA is an acronym that describes a spectrum of MRI findings including vasogenic edema and sulcal effusions (ARIA-E) and microhemorrhages (ARIA-H) and were first observed during a Phase 1 study of bapineuzumab [13] and have been observed in a number of other clinical trials with amyloid-modifying agents [14]. Interestingly, these imaging abnormalities are often clinically asymptomatic, and ARIA-E appears as a transient phenomenon [15]. Further, treatment-related ARIA seems to occur during the first weeks of therapy and the risk of ARIA decreases over time [15]. Hence, ARIA represents an intriguing phenomenon of which the clinical relevance is not yet fully understood. However, from a safety perspective, ARIA cannot be neglected and has had a profound impact on the design of clinical immunotherapy trials. Nonetheless, although

both PET imaging and histopathological studies have demonstrated that immunotherapies may reduce the amyloid burden, the exact mechanisms giving rise to ARIA remain to be fully elucidated. It has been hypothesized that the removal of vascular Aβ upon immunotherapy leads to a transient disruption of the Blood Brain Barrier (BBB) that is eventually repaired upon chronic treatment [16, 17]. Conversely, in several animal studies, Aβ immunotherapy has been associated with increased vascular amyloid deposition accompanied by increased microhemorrhages, a likely correlate to ARIA-H in humans [18]. This increased vascular Aβ may be due to an overload of an already reduced perivascular clearance pathway. Aβ clearance mechanisms are comprehensively reviewed elsewhere [19, 20]. To our knowledge, no studies have addressed the time course of such leakage events and the appearance of putative transient BBB disruptions that allow fluid, but not cells to extravasate, which would be considered equivalent of ARIA-E. In humans, ARIA-E is often anatomically associated with white matter, likely due to the prolonged accumulation of fluid along fiber tracks. The lack of extensive white matter as well as the lack of gyri and sulci in the brains of rodents [21] limits the use of T_2 weighted/fluid attenuation inversion recovery (FLAIR) sequences to monitor fluid extravasation. To better understand the relationship between Aβ immunotherapy and ARIA, three *in vivo* MRI studies were performed to study BBB impairment in a PDAPP mouse model after anti-Aβ immunization using 3D6. PDAPP mice express high levels of a familial mutation of hAPP (V717F) and progressively develop both parenchymal and vascular amyloid deposition in a region-specific manner [22]. Various histological studies in the PDAPP mouse model have shown that 3D6 treatment clears amyloid from the vascular walls with a corresponding compromise of the integrity of the vascular wall, which can result in microhemorrhages, and subsequent hemosiderin deposition [16]. In our study, to facilitate the monitoring of transient disruptions of BBB integrity that might lead to extravasation of fluids, we used a series of repeated gadolinium (Gd-DOTA)-enhanced T_1-weighted MRI scans and a T_1 mapping model [23-26] where the changes in MR signal and the estimates of the T_1-relaxation time (due to the leakage of the contrast agent) can be used both to localize BBB disruption and to assess the degree of BBB permeability.

Material and Methods

Animal Model

The PDAPP mouse model overexpresses the human amyloid precursor protein (hAPP), which successfully recapitulates several neuropathological features characteristic of AD. Many of the histological, biochemical, and structural alterations present in the PDAPP mouse closely resemble the changes found in the human AD brain [22]. Aβ deposition seen in the PDAPP mouse brain is age-dependent and region-specific. By 12 months of age, amyloid deposition is noticeable throughout the hippocampus and in the frontal region of the cortex. Between 12 and 16 months of age, an accelerated deposition is observed [27]. Female PDAPP and wild type (WT) mice (age of 12 and 16 months) were received from Taconic Biosciences (Hudson, NY – 12534, US). Female PDAPP mice were used for practical reasons, to allow the housing of multiple animals per cage (N=8 per cage). All experimental procedures were performed in accordance with European guidelines for the care and use of laboratory animals and were approved by the Committee on Animal Care and Use at the University of Antwerp, Belgium (Ethical Dossier number: 2012-33).

Experimental Study Design

In a preliminary study, we wanted to explore the feasibility of MRI to monitor vascular dynamics and BBB integrity. PDAPP (n=11) and wild type (WT) (n=11) mice (18 months old) were used. To investigate changes in BBB integrity associated with anti-Aβ immunotherapy, three independent longitudinal MRI studies were designed (Figure 1). PDAPP mice were treated with saline (_S) or the antibody 3D6 (_T), which was administered intraperitoneally, once weekly (3mg kg^{-1}, 0.5 ml). When treatment coincided with the MRI experiments, antibody was administered immediately after the imaging session. WT controls received weekly injections of saline (0.5 ml). In Study 1, PDAPP and WT mice (12 months old) were treated for 12 weeks (study 1 – *n=8 PDAPP_T; n=8 PDAPP_S; n=8 WT_S*) with T_1 MRI imaging at baseline, week 1, 4, and 12. In Study 2, PDAPP mice (12 months old) were

treated for 5 weeks (study 2 - *n=12 PDAPP_T; n=11 PDAPP_S; n=8 WT_S*). During this particular study, the dose of 3D6 was increased from 3 to 10mg kg^{-1} in week 4 and 5 to attempt to increase the number of events. In Study 3 *(n=11 PDAPP_T*), PDAPP mice (16 months old) were treated for 4 weeks. For Studies 2 and 3, MRI was performed on a weekly basis (Figure 1).

Magnetic Resonance Imaging

Animal preparation

All imaging experiments were performed on spontaneously breathing mice under isoflurane (Isoflo®, Abbot Laboratories Ltd.) anesthesia (induction 3% — maintenance 1.8%), administered in a gaseous mixture of 30% O_2 and 70% N_2. Respiration rate, monitored with a small animal respiration pad (MR-compatible Small Animal Monitoring and Gating System, SA instruments, Inc.), was maintained within normal physiological ranges. Rectal temperature was maintained at 37.0±0.2°C using a feedback coupled warm air system (MR-compatible Small Animal Heating System, SA Instruments, Inc.). To immobilize the head in a reproducible flat-skull position during the MRI experiments, mice were secured in an MRI compatible mouse stereotactic device. The head was held by a nose cone – including tooth bar – used for anesthetic gas delivery and blunt earplugs. The tail vein was cannulated with a 26-gauge needle (BD Vasculon Plus, Helsingborg, Sweden) for subsequent contrast agent injection. An actively decoupled surface array (2x2) receiver coil was positioned on top of the head. Homogeneous radiofrequency (RF) excitation was achieved using a proton volume resonator.

Magnetic resonance imaging: T_1 weighted MRI

The experiments were performed on a Bruker Pharmascan 7T imaging system with horizontal bore (Bruker, Ettlingen, Germany). For each animal, the following protocols were used after standard spectrometer adjustments (coil tune/match, RF gain calibration, shim, scout image acquisition). To

ensure uniform slice positioning, 2-dimensional coronal, axial and sagittal T_2-weighted images were acquired for each individual animal. Single slice positioning was performed in the axial plane, between bregma -1.22mm and 2.18mm. Following the slice positioning, serial sets of T_1-weighted images were continuously obtained, before (baseline T_1, pre-Gd) and every 2 minutes up to 30 minutes after (post-Gd) Gd-DOTA injection (0.2 mmol kg^{-1}; Dotarem®; Guerbet). Gd-DOTA was delivered manually and by the same experimenter. T_1-weighted images were acquired using a multiple inversion-recovery echo-planar imaging (IR-EPI) sequence with varying TIs: 28, 800, 1000, 1400, 4000, 8000ms. Following parameters were used: BW: 300 kHz; TR/TE: 10s/20.4ms; image matrix (128 x 128) (acquisition matrix: 98 x 84, zero filled read-out and partial FT phase); FOV (20 x 20) mm^2; slice thickness: 1 mm; number of averages: 2. The temporal resolution of this technique is 2 minutes.

For each time point before and after contrast administration, the T_1-values were estimated on a pixel-by-pixel basis. The measured signal intensities (SI) of the six T_1-weighted images of the IR-EPI scans were fitted to the different TI according to the 3-parameter T_1-relaxation of the spin system after an inversion pulse: $(SI(TI) = |A\text{-}B \exp(-TI/T1)| + bias$, Paravision 5.1). Manually drawn Regions of Interest (ROIs) of the left and right cortex, bilateral hippocampus and thalamus were defined by a single researcher based on a standard mouse brain atlas (Paxinos) and mean T_1 values were extracted for each of the individual ROIs and all the time points from the repeated scans (Fig 2). For each ROI, the mean baseline relaxation time is obtained from the average T_1-value of the 5 pre-Gd scans and the change of T_1 (ΔTI) versus this baseline is calculated for every time point.

Brain tissue preparation

Mice where perfused transcardially with saline, followed by approximately 20 ml of ice-cold 4% paraformaldehyde in 0.1 M PBS (pH 7.4). The whole mouse head was post-fixed overnight in 4% paraformaldehyde at 4°C prior to transfer to PBS. Brains were then processed and double-labeled for

amyloid burden and microhemorrhages. The sections were co-labeled with biotinylated 3D6 and a modified Perls' Prussian blue iron reaction for hemosiderin (NeuroSciences Associates, Knoxville, TN).

Results

T_1 mapping

BBB integrity was assessed *in vivo* using Gd-DOTA-enhanced MRI. Body weight was determined weekly to monitor general wellbeing of the mice. Overall, body weight remained constant in both PDAPP and WT animals (data not shown).

In a preliminary experiment, to assess the feasibility of our approach and prior to the administration of any treatment, we compared the impact of the Gd-DOTA injections on aged PDAPP and WT mice (18 months old). In the cortex, a much greater T_1 drop was observed in PDAPP compared to the WT mice. Since amyloid is known to accumulate in the cortical vessels first, these findings suggested that small BBB disruptions in old, untreated PDAPP mice, below the limit of visual detection, were greater than in WT animals, even before treatment is considered (Figure 3).

Next, to investigate whether the effects seen both at the individual animal level and group level were due to true leakage of the Gd-DOTA into the brain parenchyma and not related to vascular effects, the muscle tissue of the jaw, where the vasculature is naturally leaky, was included as a positive control [28]. In all the groups (PDAPP_T, PDAPP_S and WT_S), a massive drop in T_1 relaxation values (≈ 900ms) in the muscle was observed immediately after Gd-DOTA injection. Note that on T_1 weighted images, influx of Gd-DOTA was as a signal enhancement, however, after calculation of the quantitative T_1 maps, Gd-DOTA leakage into the brain was seen as a decrease in T_1 relaxation values. Following the steep initial decline, T_1 relaxation values gradually recovered in the direction of the baseline values. In the muscle, no difference was observed between the different scanning time

points (weeks). The signal in the muscle remained unchanged and was not affected by 3D6 treatment (Figure 4).

In 12 month old PDAPP and WT mice, at baseline, no differences in T_1 values were observed. After i.v. injection of Gd-DOTA, a smaller decrease in T_1 relaxation time (≈ 50ms) in the brain was observed. This was in contrast to the large drop observed in the muscle. At week 0 (pre-treatment), no differences were observed between the groups (PDAPP_T, PDAPP_S and WT_S). The average ΔT_1 for the PDAPP_T group (animals with and without active BBB disruption) doubled to -100ms while the other groups remained at ≈ -50ms. The magnitude of the drop in T_1 normalized afterwards (Figure 4).

Frequency and timing of gadolinium-enhanced signals

To document fully the observed treatment effects, bilateral ROIs of individual animals were generated for the cortex, hippocampus, and thalamus. Only the cortical ROIs demonstrated a significant impact from the Gd-DOTA, so only the cortical T_1 vs. time plots were generated. The overall effect observed in animals that received the 3D6 treatment could be ascribed to a subset of individual animals that showed markedly larger post-Gd T_1 drops (referred to as 'events'). Visual inspection of the T_1-weighted MRI images at TI= 1400ms revealed a significant increase in signal intensity after Gd-DOTA injection in the meningeal and midline area in a subset of the 3D6 treated animals. This corresponded to the areas known to first accumulate vascular Aβ deposits [16, 17] and is consistent with the hypothesis that BBB dysfunction is related to the removal of vascular amyloid (Figure 5). The increase in signal intensity was unilateral in a majority of the cases (Figure 6 – Table 1).

In the first study, a significant larger drop in T_1 in the cortex was observed in 2 PDAPP mice treated with 3D6 at week 1. After 4 weeks of treatment, one of the 2 PDAPP mice still displayed some BBB impairment. No Gd-DOTA leakage was found after 12 weeks of treatment.

In the second study, the imaging frequency was increased to a weekly scanning protocol. After 2 weeks of treatment, a significantly larger drop in T_1 relaxation values was observed in 1 animal. After 3 weeks of 3D6 treatment, the same animal and an additional animal displayed a large drop in T_1

relaxation (Figure 6). To enhance the occurrence of leakages, the dose of 3D6 was increased to 10mg/kg for the last 2 weeks (weeks 3 and 4). After the dose increase, three mice experienced somewhat smaller ΔT_1 changes of the order of 150ms – 200ms. There was 1 mouse that produced an event seen on the raw T_1 weighted images with a $\Delta T_1 < 100$ms.

Due to the temporal frequency of the MRI imaging and uncertainty regarding the evolution of a BBB event, it is unclear whether the smaller, minor events really have a lower magnitude peak or have been imaged before or after the peak enhancement effect. In the saline-treated PDAPP group, a small decrease of approximately 50ms in T_1 values compared to baseline measurements (week 0) was observed in the cortex at all time points. There was no treatment effect in the WT group.

In a third study, 16 months old PDAPP mice were treated with 3D6 and sacrificed once an event was recorded. After 1 week of treatment, 1 animal showed a major event. Immediately after scanning, the animal was sacrificed for histological analyses. Two additional animals with major events were identified after 2 weeks of treatment. These animals were also sacrificed for histological analyses.

An overview of the different studies is represented in Figure 8. Only cortical ROI's of individual animals were displayed. After treatment with 3D6 in 12 and 16 moth old PDAPP, several mice showed BBB disruption.

Histopathological analyses

Immunotherapy with the 3D6 antibody increased the occurrence of microhemorrhages (hemosiderin deposits) in leptomeningeal vessels of PDAPP mice. All the animals that showed BBB leakage by MRI were positive for Perls' Prussian bleu staining by histology (Figure 7). Hemosiderin deposition and Gd-DOTA leakage co-localized at the level of the leptomeninges.

Discussion

The present *in vivo* studies are the first to longitudinally examine the integrity of BBB following chronic treatment with the anti-Aβ antibody 3D6. To advance our understanding of the relationship between ARIA and the pathophysiology of AD, we combined Gd-DOTA enhanced T_1 MRI with histopathology to evaluate BBB integrity in PDAPP mice upon anti-Aβ immunotherapy treatment. Gd-positive signals were observed in a subset of 3D6 treated mice but not in WT or saline-treated PDAPP. Further, the temporal relationship of these BBB impairments was documented with a resolution of weekly scans. These consecutive scans indicated that the individual BBB lesions occurred early in the treatment and appeared to resolve spontaneously within a couple of days. Additionally, the risk of developing individual events seemed to diminish over a period of a few weeks.

Assessment of BBB integrity: T_1 MRI

Histological analyzes for the presence of albumin and other plasma proteins in postmortem brains have provided substantial information about BBB impairment in AD and animal models (for review see [29]). However, this evidence is mainly indirect and there is no information on the exact spatio-temporal characteristics of BBB impairment. *In vivo* detection of BBB impairment in AD has gained increased attention as these lesions might potentially contribute to cognitive dysfunction [30]. Spontaneous microbleeds in patients have been detected using T_2*-weighted imaging (based on the detection of hemosiderin substances that are paramagnetic and cause an inhomogeneity in the magnetic field). However, the relationship to histologically detected microhemorrhages is not always straightforward [31]. Following intravenous administration of superparamagnetic iron oxide (SPIO) particles, Beckman and colleagues [32] showed the feasibility of detecting CAA-related microvascular lesions in APP23 transgenic mice and demonstrated that MRI has the sensitivity to noninvasively

monitor the development of vascular pathology in transgenic mice. However, while ARIA-H has been reported in transgenic mouse models, to date only 1 publication described spontaneous appearance of ARIA-H and ARIA-E in old aged transgenic mice [33]. Additionally, until now, no well-established protocols were available to model treatment related ARIA. Gd-based MRI has been used in clinical as well as research settings to evaluate altered BBB permeability in diseases (e.g., multiple sclerosis [34] and cancer [35, 36] or injury (e.g., stroke)) [37]. After a bolus injection of Gd into the vein, the blood level of Gd rises rapidly, creating a gradient across the capillary endothelial membrane. In regions with relatively free capillary permeability, the contrast agent will leak across the vessel wall and begins to accumulate in the perivascular interstitial fluid (e.g. muscle). In the brain, the intact BBB will prevent leakage of contrast material. However, when the contrast agent leaks from the blood compartment to the brain parenchyma due to BBB disruption, the altered relaxation characteristics will be visible by T_1 MRI. Although Gd T_1 MRI has been used to probe BBB impairment in many diseases, it has not been applied extensively in AD research (for review see [38]. Recently, using an advanced dynamic contrast- enhanced MRI protocol, Montagne and colleagues [39] showed an age-dependent BBB breakdown in the hippocampus. In addition, the BBB breakdown was more pronounced in MCI patients. Moreover, BBB disruptions using DCE MRI have been shown in VCI patients [40]. However, so far, there is no convincing evidence of BBB disruption with this contrast-agent in AD, presumably due to the rapid restoration of the vascular wall. In the present study, we found that T_1 relaxation values decreased significantly in the meningeal and cortical midline area of PDAPP mice treated with 3D6. Histological analyses showed that all the animals that displayed BBB leakage visible by MRI were positive for hemosiderin by histology. Previously, it was shown that anti-Abeta antibody treatment in mouse models has been associated with increased incidence of vascular microhemorrhages, detected by hemosiderin staining [6, 17]. Zago and colleagues [16] reported histological alterations in cerebral vessels of PDAPP mice after 3D6 treatment. They showed that much of the vascular Aβ clearance occurred within the first 12 weeks of treatment (86% reduction). Hemosiderin deposits were detected in leptomeningeal vessels as early as 7 weeks after treatment. It

was suggested that leptomeningeal vessels containing vascular amyloid are predisposed to microhemorrhages during the initial phases of Aβ clearance by immunotherapy [16]. In the present study, a subset of PDAPP mice displayed a relatively steep drop in T_1 values, already after 1-2 weeks of 3D6 treatment. Histological analyses showed that all the animals that displayed BBB leakage visible by MRI were positive for hemosiderin by histology and these leakages seemed to occur in areas with apparent reduction of Aβ plaques. Interestingly, Bapineuzumab-treated subjects with ARIA-E showed greater amyloid reduction by PET imaging at week 71 [41] suggesting that BBB leakage may lead to local increase of antibody concentration and higher rate of plaque clearance. Interestingly, we only observed BBB leakages in a subset of 3D6-treated animals and not in WT or untreated PDAPP mice. Moreover, BBB leakage events occurred early in the treatment, already detectable after 1 week of immunization in a subset of animals. In addition, they seemed to be transient, and thus mimicking the pattern of the ARIA events observed in a subset of clinical trial patients [42]. Although the consequences of BBB disruption can lead to dysregulated molecular and ionic flux across the damaged BBB that can potentially culminate in neuroinflammation and neurodegeneration [30, 43], most cases of ARIA in the bapineuzumab and other anti-amyloid immunotherapy trials reported to date were clinically [15]. Symptoms, when observed, appear to be transient in nature.

Limitations of the study

The purpose of the present study was to develop a tool to visualize and quantify the extent of BBB impairment upon immunotherapy in an animal model of AD. However, these BBB disruptions likely follow the sparse nature of vascular amyloid deposition in animal models and occur focally with complex spatial patterns. ROI based analyses hampered the setting of a specific threshold on the T_1 maps because of an averaging of the T_1 values across the entire ROI, which dilutes the signal. In this respect, a voxel by voxel quantification method would be required to capture the full extent of the

BBB impairment, but given the substantial variation already present in the ROI-averaged results, it is questionable whether voxel-based analysis would increase the sensitivity or specificity. Thus both visual inspections and ROI analyses are necessary to reliably detect BBB impairment. The exact pathophysiological changes that underlie the increase in vascular permeability have yet to be fully addressed. Our results indicate that MR imaging methods with contrast agents facilitate the exploration of vascular events with unprecedented spatio-temporal resolution in animal models of amyloid-beta deposition. Additional histological and biochemical studies might shed some light on the underlying pathologies of both ARIA-H and ARIA-E.

In conclusion, with regard to the currently reported clinical experience with ARIA-H and ARIA-E in clinical trials and the preclinical work with PDAPP mice, our findings support the hypothesis that treatment with 3D6 leads to transient leakage from amyloid-laden vessels. These observations are important to increase our understanding of ARIA observed in AD patients upon Aβ lowering therapies. In addition, the current study has provided valuable insights on the time course of vascular alterations during immunization treatment, which will be useful to guide further exploration of the nature of ARIA. Finally, the developed methodology may be useful for the development of novel anti-Aβ agents and/or optimal immunotherapy dosing strategies that minimize vascular responses.

Acknowledgements

This study was sponsored by Janssen Alzheimer Immunotherapy R&D. Wagner Zago was an employee of Janssen Alzheimer Immunotherapy R&D at the beginning of study and is now employee of Prothena Biosciences Inc. This research was also supported by the European Union's Seventh Framework Programme under grant agreement number 278850 (INMiND). The Bruker Pharmascan 7T system (Bruker, Ettlingen, Germany) was purchased through Hercules foundation funding (Belgium) under the promoter-ship of Prof. dr. Annemie Van der Linden. Caroline Guglielmetti is holder of an IWT PhD fellowship (agency for innovation by Science and Technology).

References

[1] Karran E, Mercken M, De Strooper B (2011) The amyloid cascade hypothesis for Alzheimer's disease: an appraisal for the development of therapeutics. *Nat Rev Drug Discov* **10**, 698-712.

[2] Schenk D, Barbour R, Dunn W, Gordon G, Grajeda H, Guido T, Hu K, Huang J, Johnson-Wood K, Khan K, Kholodenko D, Lee M, Liao Z, Lieberburg I, Motter R, Mutter L, Soriano F, Shopp G, Vasquez N, Vandevert C, Walker S, Wogulis M, Yednock T, Games D, Seubert P (1999) Immunization with amyloid-beta attenuates Alzheimer-disease-like pathology in the PDAPP mouse. *Nature* **400**, 173-177.

[3] Janus C, Pearson J, McLaurin J, Mathews PM, Jiang Y, Schmidt SD, Chishti MA, Horne P, Heslin D, French J, Mount HT, Nixon RA, Mercken M, Bergeron C, Fraser PE, St George-Hyslop P, Westaway D (2000) A beta peptide immunization reduces behavioural impairment and plaques in a model of Alzheimer's disease. *Nature* **408**, 979-982.

[4] Morgan D, Diamond DM, Gottschall PE, Ugen KE, Dickey C, Hardy J, Duff K, Jantzen P, DiCarlo G, Wilcock D, Connor K, Hatcher J, Hope C, Gordon M, Arendash GW (2000) A beta peptide vaccination prevents memory loss in an animal model of Alzheimer's disease. *Nature* **408**, 982-985.

[5] Bard F, Cannon C, Barbour R, Burke RL, Games D, Grajeda H, Guido T, Hu K, Huang J, Johnson-Wood K, Khan K, Kholodenko D, Lee M, Lieberburg I, Motter R, Nguyen M, Soriano F, Vasquez N, Weiss K, Welch B, Seubert P, Schenk D, Yednock T (2000) Peripherally administered antibodies against amyloid beta-peptide enter the central nervous system and reduce pathology in a mouse model of Alzheimer disease. *Nat.Med.* **6**, 916-919.

[6] Wilcock DM, Rojiani A, Rosenthal A, Subbarao S, Freeman MJ, Gordon MN, Morgan D (2004) Passive immunotherapy against Abeta in aged APP-transgenic mice reverses cognitive deficits and depletes parenchymal amyloid deposits in spite of increased vascular amyloid and microhemorrhage. *J.Neuroinflammation.* **1**, 24.

[7] Masliah E, Hansen L, Adame A, Crews L, Bard F, Lee C, Seubert P, Games D, Kirby L, Schenk D (2005) Abeta vaccination effects on plaque pathology in the absence of encephalitis in Alzheimer disease. *Neurology* **64**, 129-131.

[8] Boche D, Zotova E, Weller RO, Love S, Neal JW, Pickering RM, Wilkinson D, Holmes C, Nicoll JA (2008) Consequence of Abeta immunization on the vasculature of human Alzheimer's disease brain. *Brain* **131**, 3299-3310.

[9] Zago W, Buttini M, Comery TA, Nishioka C, Gardai SJ, Seubert P, Games D, Bard F, Schenk D, Kinney GG (2012) Neutralization of soluble, synaptotoxic amyloid beta species by antibodies is epitope specific. *J Neurosci* **32**, 2696-2702.

[10] Salloway S, Sperling R, Brashear HR (2014) Phase 3 trials of solanezumab and bapineuzumab for Alzheimer's disease. *N Engl J Med* **370**, 1460.

[11] Ostrowitzki S, Deptula D, Thurfjell L, Barkhof F, Bohrmann B, Brooks DJ, Klunk WE, Ashford E, Yoo K, Xu ZX, Loetscher H, Santarelli L (2012) Mechanism of amyloid removal in patients with Alzheimer disease treated with gantenerumab. *Arch Neurol* **69**, 198-207.

[12] Sperling RA, Jack CR, Jr., Black SE, Frosch MP, Greenberg SM, Hyman BT, Scheltens P, Carrillo MC, Thies W, Bednar MM, Black RS, Brashear HR, Grundman M, Siemers ER, Feldman HH, Schindler RJ (2011) Amyloid-related imaging abnormalities in amyloid-modifying therapeutic trials: recommendations from the Alzheimer's Association Research Roundtable Workgroup. *Alzheimers Dement* **7**, 367-385.

[13] Black RS, Sperling RA, Safirstein B, Motter RN, Pallay A, Nichols A, Grundman M (2010) A single ascending dose study of bapineuzumab in patients with Alzheimer disease. *Alzheimer Dis Assoc Disord* **24**, 198-203.

[14] Moreth J, Mavoungou C, Schindowski K (2013) Passive anti-amyloid immunotherapy in Alzheimer's disease: What are the most promising targets? *Immun Ageing* **10**, 18.

[15] Sperling R, Salloway S, Brooks DJ, Tampieri D, Barakos J, Fox NC, Raskind M, Sabbagh M, Honig LS, Porsteinsson AP, Lieberburg I, Arrighi HM, Morris KA, Lu Y, Liu E, Gregg KM,

Brashear HR, Kinney GG, Black R, Grundman M (2012) Amyloid-related imaging abnormalities in patients with Alzheimer's disease treated with bapineuzumab: a retrospective analysis. *Lancet Neurol.* **11**, 241-249.

[16] Zago W, Schroeter S, Guido T, Khan K, Seubert P, Yednock T, Schenk D, Gregg KM, Games D, Bard F, Kinney GG (2013) Vascular alterations in PDAPP mice after anti-Abeta immunotherapy: Implications for amyloid-related imaging abnormalities. *Alzheimers.Dement.*

[17] Schroeter S, Khan K, Barbour R, Doan M, Chen M, Guido T, Gill D, Basi G, Schenk D, Seubert P, Games D (2008) Immunotherapy reduces vascular amyloid-beta in PDAPP mice. *J.Neurosci.* **28**, 6787-6793.

[18] Wilcock DM, Colton CA (2009) Immunotherapy, vascular pathology, and microhemorrhages in transgenic mice. *CNS Neurol Disord Drug Targets* **8**, 50-64.

[19] Weller RO, Subash M, Preston SD, Mazanti I, Carare RO (2008) Perivascular drainage of amyloid-beta peptides from the brain and its failure in cerebral amyloid angiopathy and Alzheimer's disease. *Brain Pathol* **18**, 253-266.

[20] Zlokovic BV, Deane R, Sagare AP, Bell RD, Winkler EA (2010) Low-density lipoprotein receptor-related protein-1: a serial clearance homeostatic mechanism controlling Alzheimer's amyloid beta-peptide elimination from the brain. *J Neurochem* **115**, 1077-1089.

[21] Rakic P (2009) Evolution of the neocortex: a perspective from developmental biology. *Nat Rev Neurosci* **10**, 724-735.

[22] Games D, Adams D, Alessandrini R, Barbour R, Berthelette P, Blackwell C, Carr T, Clemens J, Donaldson T, Gillespie F, et al. (1995) Alzheimer-type neuropathology in transgenic mice overexpressing V717F beta-amyloid precursor protein. *Nature* **373**, 523-527.

[23] Harris NG, Gauden V, Fraser PA, Williams SR, Parker GJ (2002) MRI measurement of blood-brain barrier permeability following spontaneous reperfusion in the starch microsphere model of ischemia. *Magn Reson.Imaging* **20**, 221-230.

[24] Lund H, Krakauer M, Skimminge A, Sellebjerg F, Garde E, Siebner HR, Paulson OB, Hesse D, Hanson LG (2013) Blood-brain barrier permeability of normal appearing white matter in relapsing-remitting multiple sclerosis. *PLoS One* **8**, e56375.

[25] Essig M, Dinkel J, Gutierrez JE (2012) Use of contrast media in neuroimaging. *Magn Reson Imaging Clin N Am* **20**, 633-648.

[26] van Vliet EA, Otte WM, Gorter JA, Dijkhuizen RM, Wadman WJ (2014) Longitudinal assessment of blood-brain barrier leakage during epileptogenesis in rats. A quantitative MRI study. *Neurobiol Dis* **63**, 74-84.

[27] Johnson-Wood K, Lee M, Motter R, Hu K, Gordon G, Barbour R, Khan K, Gordon M, Tan H, Games D, Lieberburg I, Schenk D, Seubert P, McConlogue L (1997) Amyloid precursor protein processing and A beta42 deposition in a transgenic mouse model of Alzheimer disease. *Proc Natl Acad Sci U S A* **94**, 1550-1555.

[28] Montagne A, Toga AW, Zlokovic BV (2016) Blood-Brain Barrier Permeability and Gadolinium: Benefits and Potential Pitfalls in Research. *JAMA Neurol* **73**, 13-14.

[29] Bowman GL, Quinn JF (2008) Alzheimer's disease and the Blood-Brain Barrier: Past, Present and Future. *Aging health* **4**, 47-55.

[30] Erickson MA, Banks WA (2013) Blood-brain barrier dysfunction as a cause and consequence of Alzheimer's disease. *J Cereb Blood Flow Metab* **33**, 1500-1513.

[31] Greenberg SM, Vernooij MW, Cordonnier C, Viswanathan A, Al-Shahi Salman R, Warach S, Launer LJ, Van Buchem MA, Breteler MM, Microbleed Study G (2009) Cerebral microbleeds: a guide to detection and interpretation. *Lancet Neurol* **8**, 165-174.

[32] Beckmann N, Gerard C, Abramowski D, Cannet C, Staufenbiel M (2011) Noninvasive magnetic resonance imaging detection of cerebral amyloid angiopathy-related microvascular alterations using superparamagnetic iron oxide particles in APP transgenic mouse models of Alzheimer's disease: application to passive Abeta immunotherapy. *J Neurosci* **31**, 1023-1031.

[33] Goodman JF, G.;, Angus W.; Brown, T.; Cheng-te Chou, P.; Bales, K. (2012) in *Alzheimer's & Dementia*, p. 2.

[34] Simon JH (1997) Contrast-enhanced MR imaging in the evaluation of treatment response and prediction of outcome in multiple sclerosis. *J.Magn Reson.Imaging* **7**, 29-37.

[35] Helbich TH, Roberts TP, Gossmann A, Wendland MF, Shames DM, Adachi M, Yang S, Huber S, Daldrup H, Brasch RC (2000) Quantitative gadopentetate-enhanced MRI of breast tumors: testing of different analytic methods. *Magn Reson.Med.* **44**, 915-924.

[36] Kaiser WA, Zeitler E (1989) MR imaging of the breast: fast imaging sequences with and without Gd-DTPA. Preliminary observations. *Radiology* **170**, 681-686.

[37] Maeda M, Maley JE, Crosby DL, Quets JP, Zhu MW, Lee GJ, Lawler GJ, Ueda T, Bendixen BH, Yuh WT (1997) Application of contrast agents in the evaluation of stroke: conventional MR and echo-planar MR imaging. *J.Magn Reson.Imaging* **7**, 23-28.

[38] van de Haar HJ, Burgmans S, Hofman PA, Verhey FR, Jansen JF, Backes WH (2015) Blood-brain barrier impairment in dementia: current and future in vivo assessments. *Neurosci Biobehav Rev* **49**, 71-81.

[39] Montagne A, Barnes SR, Sweeney MD, Halliday MR, Sagare AP, Zhao Z, Toga AW, Jacobs RE, Liu CY, Amezcua L, Harrington MG, Chui HC, Law M, Zlokovic BV (2015) Blood-brain barrier breakdown in the aging human hippocampus. *Neuron* **85**, 296-302.

[40] Taheri S, Gasparovic C, Huisa BN, Adair JC, Edmonds E, Prestopnik J, Grossetete M, Shah NJ, Wills J, Qualls C, Rosenberg GA (2011) Blood-brain barrier permeability abnormalities in vascular cognitive impairment. *Stroke* **42**, 2158-2163.

[41] Liu EW, D.; Sperling, R.; Salloway, S.; Fox, N.; Blennow, K.; Scheltens, P.; Schmidt, M.E.; Streffer, J.; Novak, G.; Einstein, S.; Boorh, K.; Ketter, N.; Brashear,H.R. (2015) in *The 12th international conference on Alzheimer's & Parkinson's diseases 2015*, Nice, France.

[42] Salloway S, Sperling R, Gilman S, Fox NC, Blennow K, Raskind M, Sabbagh M, Honig LS, Doody R, van Dyck CH, Mulnard R, Barakos J, Gregg KM, Liu E, Lieberburg I, Schenk D, Black R,

Grundman M, Bapineuzumab 201 Clinical Trial I (2009) A phase 2 multiple ascending dose trial of bapineuzumab in mild to moderate Alzheimer disease. *Neurology* **73**, 2061-2070.

[43] Obermeier B, Daneman R, Ransohoff RM (2013) Development, maintenance and disruption of the blood-brain barrier. *Nat Med* **19**, 1584-1596.

Study#	Treatment group	Number of T1 events						Cumulative	
		W0	**W1**	**W4**	**W12**				
Study1	WT	0/8	0/8	0/7	0/6			0/8	0%
	PDAPP - saline	0/8	0/7	0/7	0/4			0/8	0%
	PDAPP - 3D6 (3mg/kg)	0/8	2/7	1/6	0/6			3/8	**38%**
		W0	**W1**	**W2**	**W3**	**W4***	**W5***		
Study2	WT	0/8	0/8	0/8	0/8				
	PDAPP - saline	0/11	0/11	0/11	0/11	0/11	0/11	0/11	0%
	PDAPP - 3D6 (3 or 10*mg/kg)	0/12	0/12	1/12	2/12	3/12	3/11	5/12	**41%**
		W0	**W1**	**W2**	**W3**	**W4**			
Study3	PDAPP - 3D6 (3mg/kg)	0/11	1/11	2/10	1/7	0/5		4/11	**36%**

513

514 **Table 1: Overview different individual events of treated PDAPP mice of the three independent**

515 **treatment studies.** Multiple events could be observed in the same animal during treatment (# *).

516

517

518

519

520

521

522

523

524

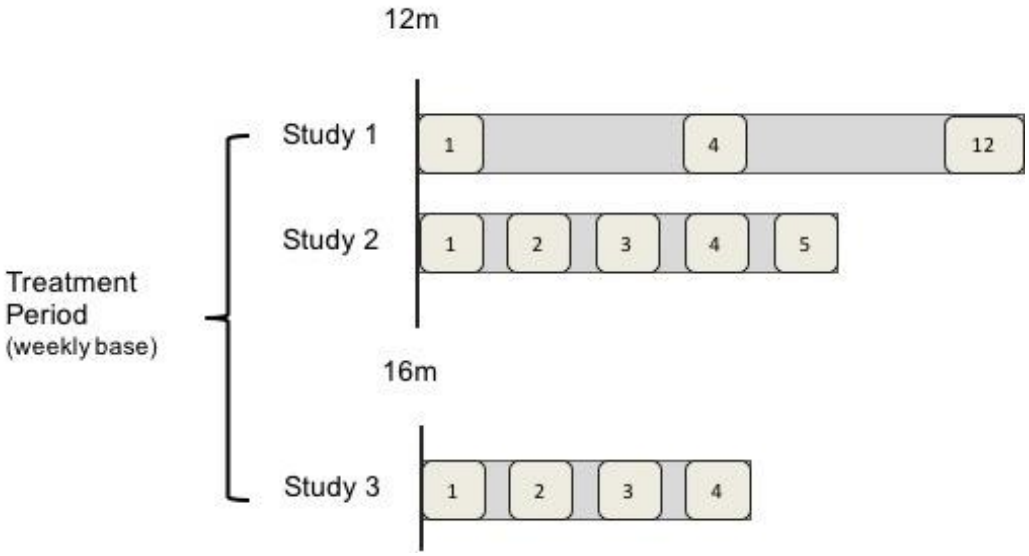

Figure 1: **Study design**. At **12 months of age**, PDAPP mice were injected with 3D6 or saline. **Study 1** (n=8 PDAPP_T; n=8 PDAPP_S; n=8 WT), treatment for 12 weeks (dose 3 mg/kg/week) and **study 2** (n=12 PDAPP_T; n=8 WT; n=12 PDAPP_S)], treatment for 5 weeks (dose 3 mg/kg/week for the first 3 weeks – 10 mg/kg/week for the last 2 weeks). WT controls received weekly an injection with saline. In **study 3** (n=12 PDAPP_T), PDAPP mice at the **age of 16 months** were weekly injected with 3 mg/kg/week of 3D6 for a period of 4 weeks. In study 1, MRI was performed after 1, 4 and 12 weeks of treatment. In the second and third study, MRI was performed on a weekly basis.

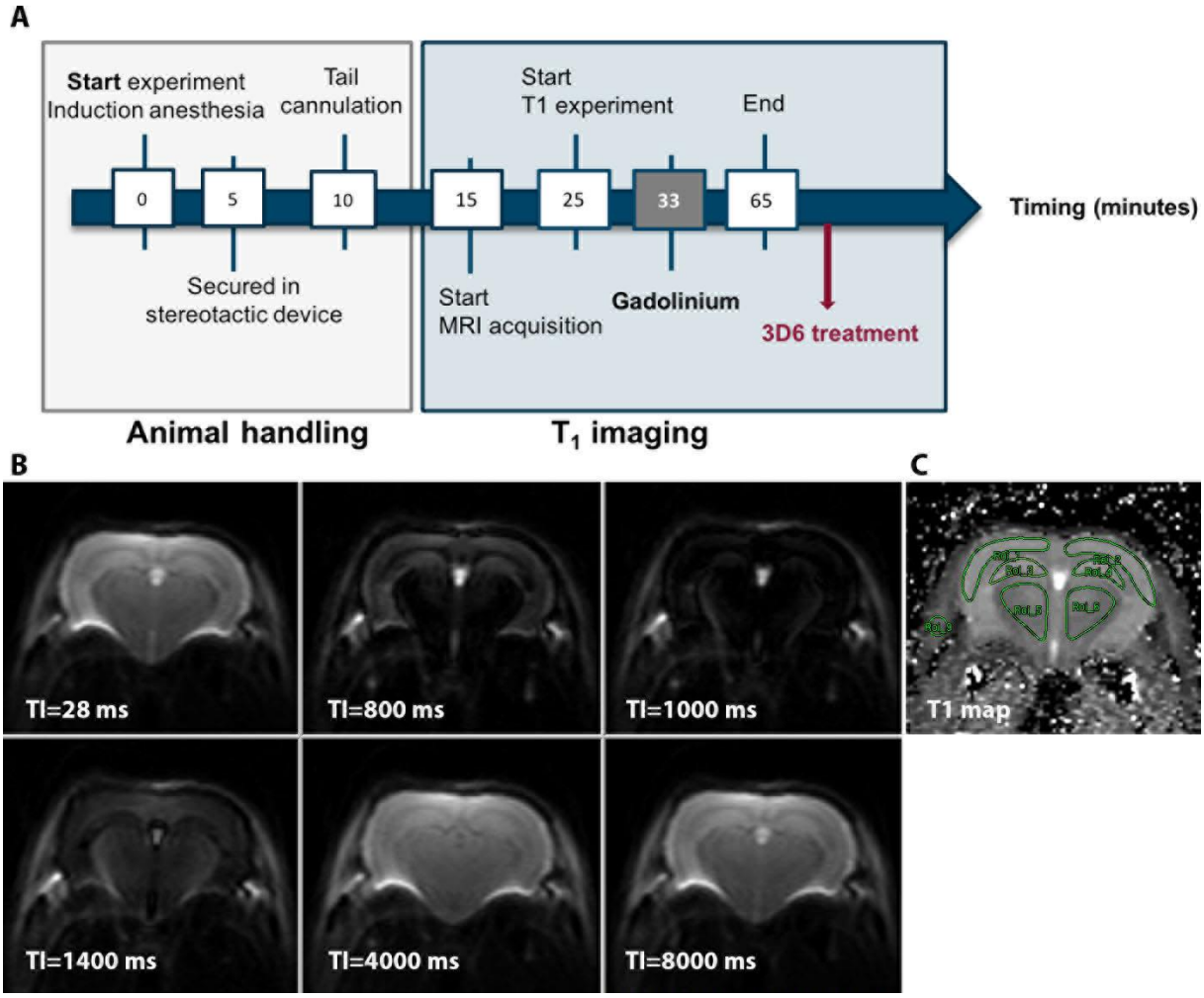

Figure 2: **Experimental design.** (A) T_1 weighted images (acquired every 2 minutes) were obtained to investigate BBB integrity, before (baseline T_1) and after administration of Gd-DOTA (0.2 mmol/ kg). Injections were delivered manually. T_1 weighted images were acquired using a multiple inversion-recovery echo-planar imaging (EPI) sequence. 3D6 treatment was done on a weekly basis for all three independent studies. When the treatment coincided with the MRI imaging, injections of 3D6 were done after the imaging session. (B) Representative multiple inversion recovery T_1 weighted images with different inversion time (ranging from 28 ms to 8000 ms). The contrast changes due to varying the TI. (C) These images were used to calculate the quantitative T_1 maps (using a mono-exponential fit). This T_1 map was used to extract the T_1 values from the different brain structures. Paxinos ROI's used for T_1 analyses are illustrated on a calculated T_1 map. (ROI 1-2: cortex; ROI 3-4: hippocampus; ROI 5-6: thalamus; ROI 7: muscle).

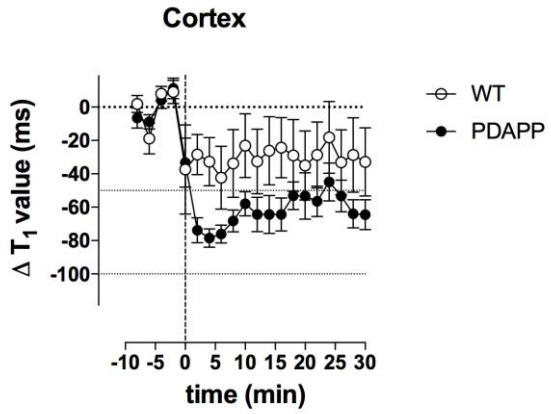

546

547 **Figure 3**: **T_1 graphs displaying ΔT_1 values of 18 months old PDAPP and WT mice, without**
548 **immunization treatment.** In a preliminary experiment, non-treated PDAPP and WT mice were
549 injected with GD-DOTA. The T_1 time course values show a greater reduction of T_1 relaxation values in
550 the PDAPP mouse brains, suggesting that these animals have greater BBB permeability, even before
551 treatment is applied.

552

553

554

555

556

557

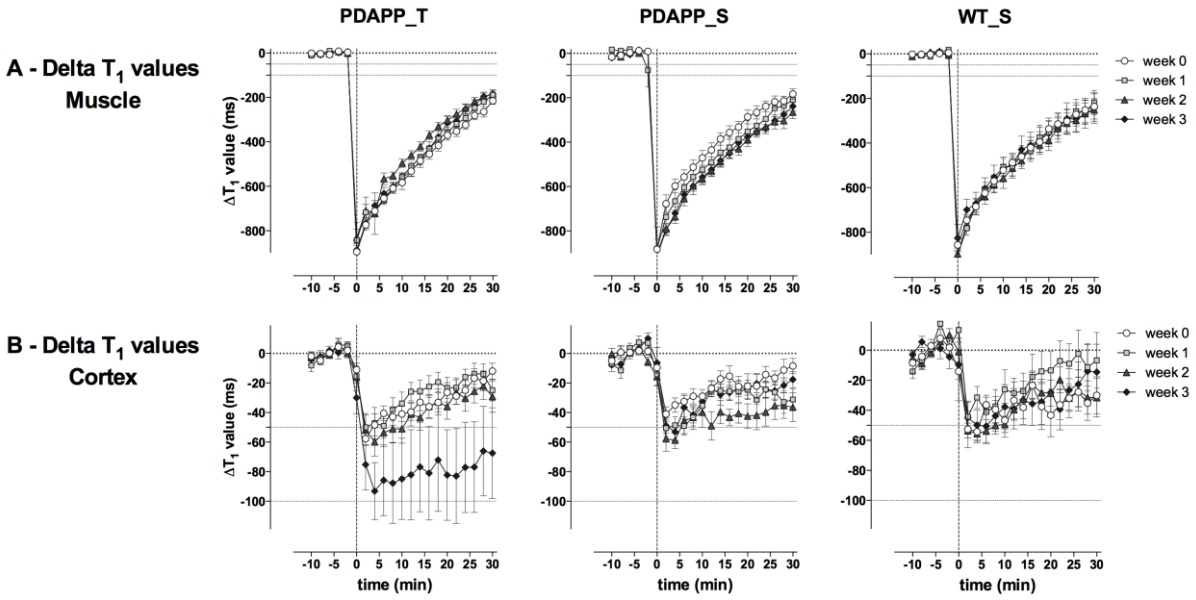

Figure 4: **T_1 graphs displaying ΔT_1 values before and after injection of Gd (t = 0) in 12 months old mice** (study 2). The cortex (A) showed a smaller reduction in T_1 due to the presence of the BBB ($\Delta T_1 \approx$ -50ms) compared to the muscle (B) without a BBB ($\Delta T_1 \approx$ -900ms). At week 0 (pre-treatment), no differences were observed between the groups (PDAPP_T (3D6-treated), PDAPP_S (saline-treated) and WT_S (saline-treated). No differences in cortical T_1 values were observed at baseline. The average initial ΔT_1 for the PDAPP 3D6 group (animals with and without active BBB disruption) after 3 weeks of treatment doubled to -100ms while the drop for the other groups remained at ≈ -50ms. The signal in the muscle remained unchanged after the treatment regime.

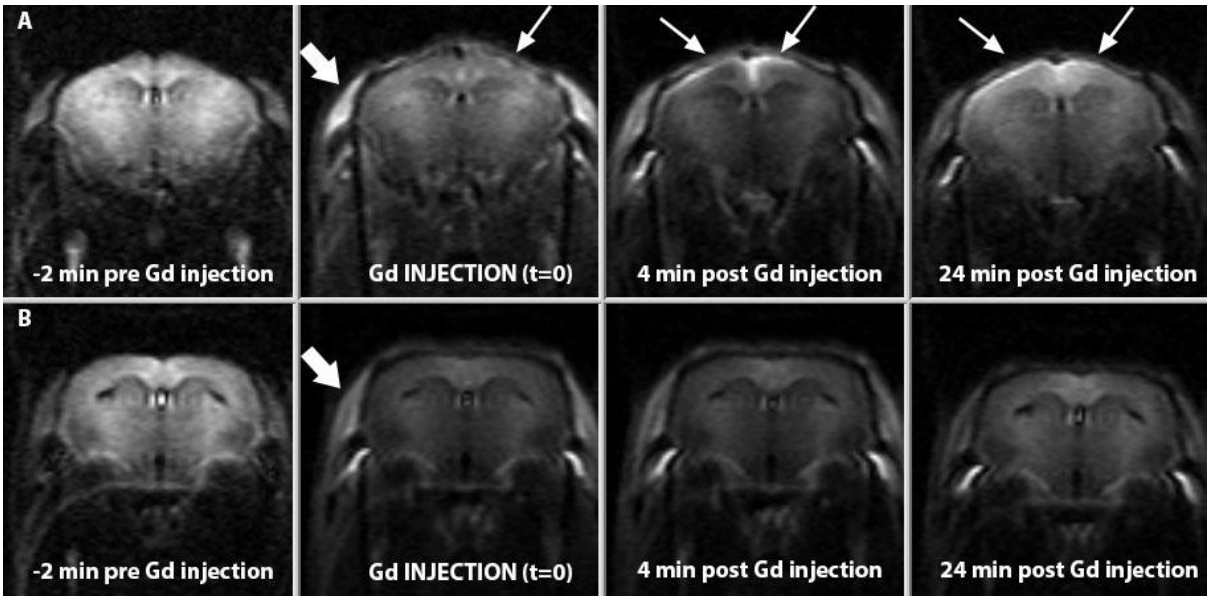

Figure 5: T_1 weighted images of TI = 1400ms from different frames pre-Gd-DOTA (-2 min), during Gd-DOTA injection (t=0) and 4 and 24 min post Gd-DOTA injection. Each scan frame was acquired in a period of 2 minutes. The images in (A) show the enhancement pattern for a PDAPP animal that was experiencing an active BBB disruption event (thin arrows), a hyper-intensity that was predominately occurring in the left cortical and medial right cortical ROI. The images in (B) were acquired from a treated PDAPP animal that does not demonstrated BBB dysfunction since no contrast enhancement was detected. Also note the enhancement of the muscle, indicated by the thicker arrows in both (A) and (B).

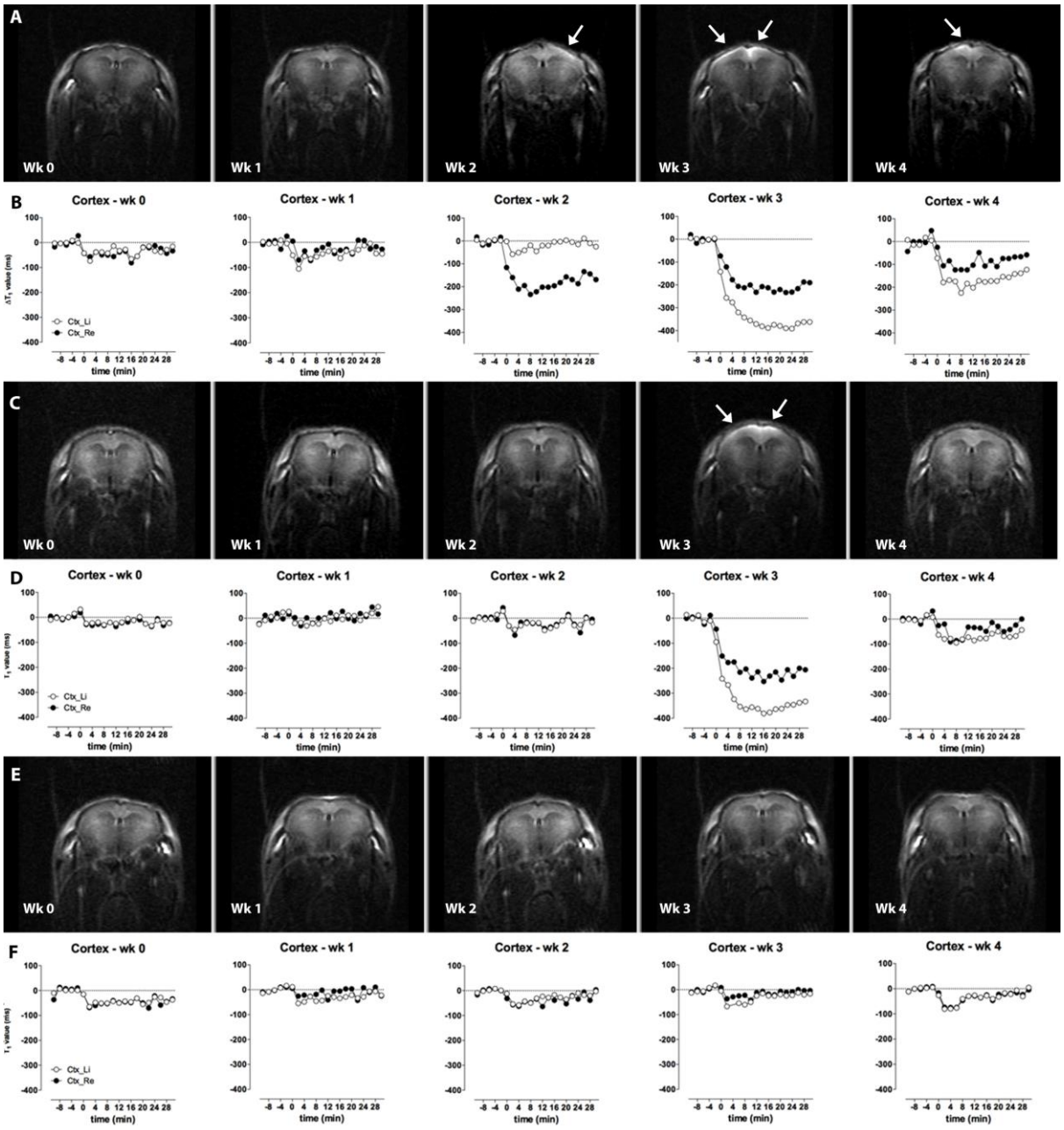

589

590 **Figure 6: T_1-weighted images (TI=1400 ms) and time course curves of weeks 1 – 4 post treatment**.
591 T_1 values were derived from cortical ROIs (left & right) of the T_1 maps of two representative PDAPP
592 animals treated with 3D6 (A-D) and saline (E-F) (study 2). BBB leakage events occurred at weeks 2, 3,
593 4 and can be seen on T_1-weighted images as a signal enhancement in the cortical area. After
594 calculation of the T_1 maps – based on the T_1 images – Gd-DOTA leakages into the brain was seen as a
595 drop in T_1 relaxation values (ms) (A, C) (white arrows). The time courses of the individual cortical ROIs
596 (week 0 - 4) illustrate the asymmetry and support the effects seen on the images. The non-

597 overlapping enhancement patterns in weeks 2, 3 and 4, imply independent events, suggesting that
598 the initiation, evolution and resolution of a BBB event occurred ≤ 1 week.
599
600
601
602
603
604
605
606
607
608
609
610
611
612
613
614
615
616
617
618
619
620
621
622

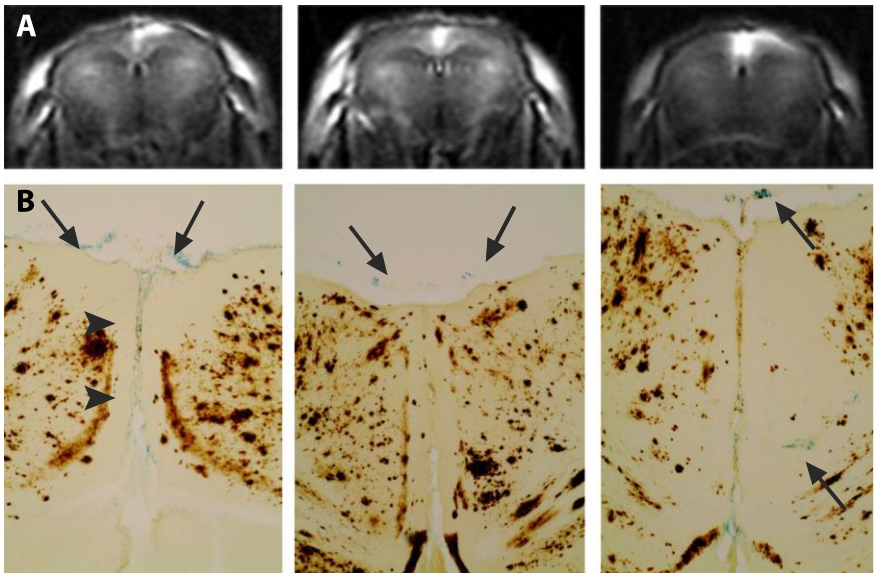

Figure 7: Histopathology compared to MRI. (A) *in vivo* T_1 weighted images of individual PDAPP mice displaying Gd-enhancement on the T_1 weighted (IT: 1400ms) image. (B) Corresponding coronal brain sections stained for amyloid burden using a biotinylated 3D6 antibody (brown) and microhemorrhages using Perls' Prussian bleu stain (blue) of the corresponding PDAPP mouse. Microhemorrhages were observed predominantly in the leptomeninges vessels and co-localized with MRI events.

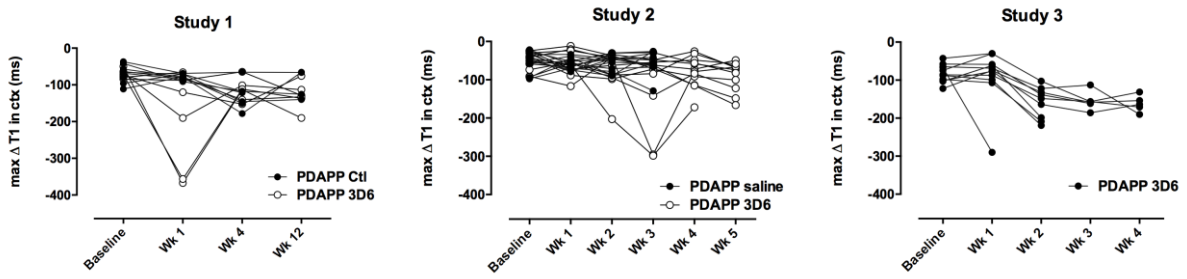

641

642 **Figure 8**: Data points (circles) represent maximal T_1 drops (between +4 and +6 min after Gd-DOTA
643 injection) in the cortex of individual animals in study 1, study 2 and study 3. After treatment with 3D6
644 in 12 and 16 moth old PDAPP, several mice showed BBB disruption. A clear delineation of ΔT_1 is seen
645 compared with non-treated PDAPP animals. Note: these are averaged data of left and right cortical
646 area. Furthermore, these T_1 decreases developed and recovered within the temporal resolution of
647 the study. What is not appreciated from the curves is that the increased changes in T_1 preceding and
648 following the maximum T_1 decline are actually different BBB events. These curves suggest that one
649 might be able to define an event threshold based solely on ΔT_1. However, the situation is less
650 straightforward and more analysis is needed before a cutoff or other criteria can be determined.

651